Large reduction of thermal conductivity leading to enhanced thermoelectric performance in p-type Mg_3Bi_2-$YbMg_2Bi_2$ solid solutions

Journal:	*Journal of Materials Chemistry C*
Manuscript ID	TC-ART-10-2018-005424.R1
Article Type:	Paper
Date Submitted by the Author:	10-Dec-2018
Complete List of Authors:	Zhou, Ting; University of Electronic Science and Technology of China, College of Electronic Science and Engineering Mao, Jun; University of Houston, Physics Jiang, Jing; University of Electronic Science and Technology of China, College of Electronic Science and Engineering Song, Shaowei ; University of Houston, Material Science and Engineering Zhu, Hangtian; University of Houston Zhu, Qing; University of Houston Zhang, Qinyong; Xihua University, Center for Advanced Materials & Energy Ren, Wuyang; University of Electronic Science and Technology of China, State Key Lab Elect Thin Films & Integrated Devic Wang, Zhiming; University of Electronic Science and Technology of China, Wang, Chao; University of Electronic Science and Technology of China, College of Electronic Science and Engineering Ren, Zhifeng ; University of Houston, Physics

Journal Name

ARTICLE

Large reduction of thermal conductivity leading to enhanced thermoelectric performance in p-type Mg_3Bi_2-$YbMg_2Bi_2$ solid solutions

Received 00th January 20xx,
Accepted 00th January 20xx

DOI: 10.1039/x0xx00000x

www.rsc.org/

Ting Zhou,[ab] Jun Mao,[b] Jing Jiang,[a] Shaowei Song,[b] Hangtian Zhu,[b] Qing Zhu,[b] Qinyong Zhang,[c] Wuyang Ren,[bd] Zhiming Wang,[d] Chao Wang,*[a] Zhifeng Ren*[b]

Intensifying the phonon scattering *via* point defect engineering has been demonstrated to be particularly effective in minimizing the lattice thermal conductivity for enhancing thermoelectric performance. In this work, significant phonon scattering has been realized by alloying $YbMg_2Bi_2$ with Mg_3Bi_2. The substantial mass difference between the host atom Yb and the alloying atom Mg leads to an intense phonon scattering effect that significantly reduces the lattice thermal conductivity. The room-temperature lattice thermal conductivity decreases from ~2.7 W m^{-1} K^{-1} for $YbMg_2Bi_{1.96}$ to ~0.8 W m^{-1} K^{-1} for $Yb_{0.7}Mg_{0.3}Mg_2Bi_{1.96}$, a reduction of ~70%. Benefiting from the greatly reduced thermal conductivity, the average *ZT* has been effectively improved from ~0.46 for $YbMg_2Bi_{1.96}$ to ~0.61 for $Yb_{0.8}Mg_{0.2}Mg_2Bi_{1.96}$, an enhancement of ~33%. In addition, the predicted maximum heat-to-electricity conversion efficiency can be increased from ~7% for $YbMg_2Bi_{1.96}$ to ~10% for $Yb_{0.8}Mg_{0.2}Mg_2Bi_{1.96}$.

Introduction

Thermoelectric materials have attracted extensive interest in the last several decades due to their capability of converting waste heat into electricity. As the main challenge preventing the widespread use of thermoelectrics is their low conversion efficiency, improving the heat-to-electricity conversion efficiency is particularly critical.[1-4] The thermoelectric energy conversion efficiency of a material is determined by the Carnot efficiency and the material's dimensionless thermoelectric figure of merit (*ZT*), defined as $ZT=S^2\sigma T/\kappa$, where *S*, σ, κ, and *T* are the Seebeck coefficient, electrical conductivity, thermal conductivity, and absolute temperature, respectively. Total thermal conductivity contains the lattice, electronic, and bipolar contributions: $\kappa_{total}=\kappa_L+\kappa_e+\kappa_B$. Therefore, a good thermoelectric material with a high *ZT* should have a high Seebeck coefficient, high electrical conductivity and low thermal conductivity.

Thus far, high *ZT*s have been reported in several classes of bulk thermoelectric materials, such as half-Heuslers[5-7], lead telluride[8, 9], bismuth telluride[10, 11], and Zintls[12-14]. Among these thermoelectric materials, Zintl phase compounds are highly promising due to their complex crystal structures along with their large numbers of atoms per unit cell.[15, 16] Zintl compounds contain the covalently bonded networks of complex anions or metalloids ("electron-crystal" electronic structure) and cations ("phonon-glass" characteristic).[13, 14] A variety of high-performance Zintl phases, such as $Yb_{14}MnSb_{11}$[17-20], $Mg_{3+x}Sb_{1.5}Bi_{0.5}$[21-27], AZn_2Sb_2 (A = Sr, Ca, Yb, or Eu)[15, 28-33], $BaGa_2Sb_2$,[34, 35] and $A_5M_2Sb_6$ (A = Ca, or Yb; M = Al, Ga, or In)[36-40], have been studied for potential thermoelectric applications. In addition to the Sb-based Zintl compounds, thermoelectric properties of the analogous Bi-based compounds have also been investigated.[41-47] Enhanced thermoelectric performance of Bi-based materials has been realized by alloying $YbMg_2Bi_2$ with $EuMg_2Bi_2$ and $CaMg_2Bi_2$. Substitution of isoelectronic ions introduces disorder to scatter phonons without significantly disrupting the electrical conductivity.[14] This is a highly effective method to improve the thermoelectric performance of many other materials as well.[48-53] It has been reported that $YbMg_2Bi_2$ has good thermoelectric performance but with relatively high lattice thermal conductivity. Therefore, it is possible to further improve the thermoelectric performance of $YbMg_2Bi_2$ by reducing the lattice thermal conductivity via phonon engineering, *e.g.*, alloying $YbMg_2Bi_2$ with Mg_3Bi_2 (for a larger mass difference in the cationic site). In addition, it should be noted that the pure phase of any AB_2M_2 (A = Ca, Ba, Sr, Yb, or Eu; B = Mn, Zn, or Cd; M = Sb or Bi) Zintl compound, which is crucial for the high thermoelectric performance, is not easily obtainable since the A or B in AB_2M_2 vaporizes or reacts with the reaction container.[31, 44] Therefore, optimizing the composition to obtain a high quality specimen can effectively improve the thermoelectric performance.

[a] *State Key Laboratory of Electronic Thin Films and Integrated Devices, School of Electronic Science and Engineering, University of Electronic Science and Technology of China, Chengdu 611731, China. *E-mail: cwang@uestc.edu.cn*
[b] *Department of Physics and TcSUH, University of Houston, Houston, Texas 77204, United States. *E-mail: zren@uh.edu*
[c] *Key Laboratory of Fluid and Power Machinery of Ministry of Education, Center for Advanced Materials and Energy, Xihua University, Chengdu 610039, China.*
[d] *Institute of Fundamental and Frontier Sciences, University of Electronic Science and Technology of China, Chengdu 610054, China.*

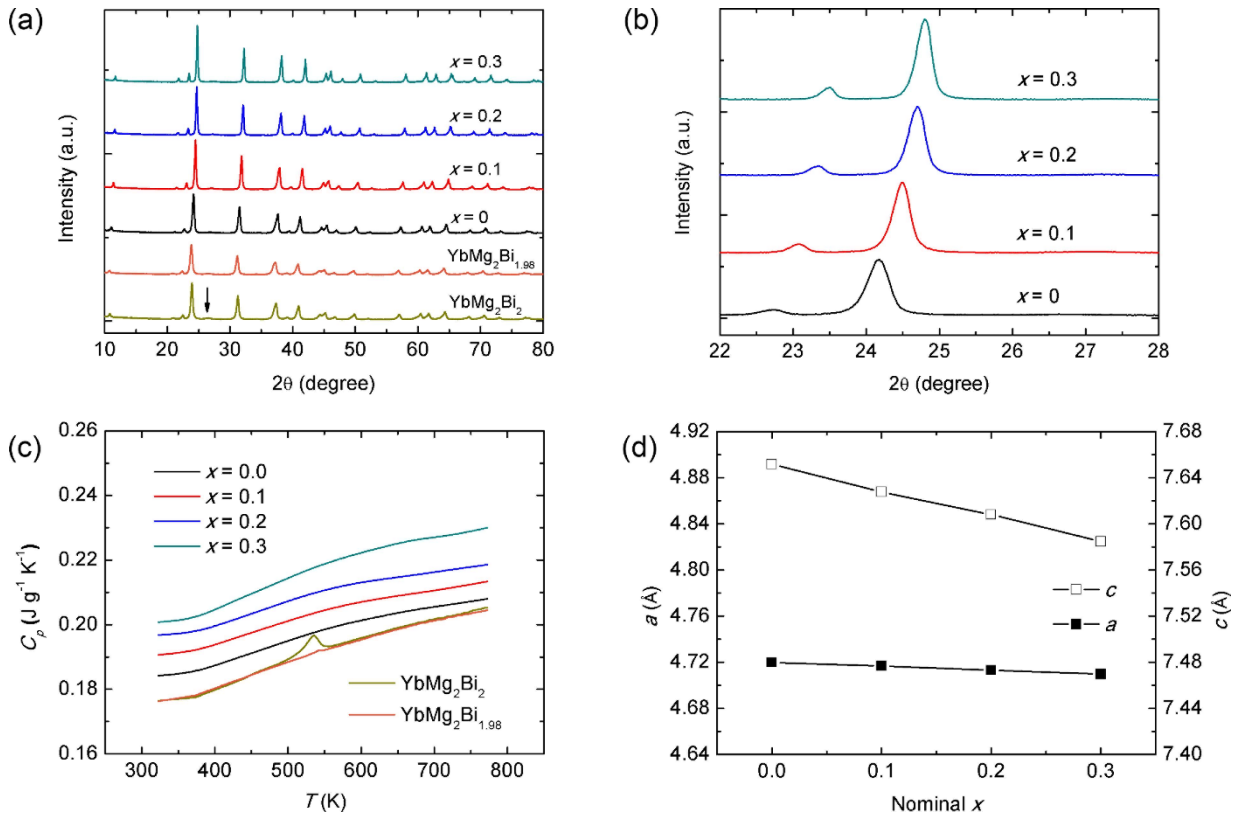

Fig. 1 (a) XRD patterns of $YbMg_2Bi_2$, $YbMg_2Bi_{1.98}$, and $Yb_{1-x}Mg_xMg_2Bi_{1.96}$ (x = 0, 0.1, 0.2, and 0.3) and (b) zoomed-in XRD patterns of $Yb_{1-x}Mg_xMg_2Bi_{1.96}$ (x = 0, 0.1, 0.2, and 0.3) between 22° and 28°; (c) temperature-dependent heat capacity of $YbMg_2Bi_2$, $YbMg_2Bi_{1.98}$, and $Yb_{1-x}Mg_xMg_2Bi_{1.96}$ (x = 0, 0.1, 0.2, and 0.3); and (d) dependence of lattice parameters on composition for $Yb_{1-x}Mg_xMg_2Bi_{1.96}$.

Therefore, the motivation for this work is first to achieve the pure-phase specimen of $YbMg_2Bi_2$ by optimization of the composition. Afterwards, in order to further improve the thermoelectric properties of the $YbMg_2Bi_2$-based materials, solid solutions between the pure-phase $YbMg_2Bi_2$ and Mg_3Bi_2 are prepared. Our results show that the room-temperature lattice thermal conductivity of $YbMg_2Bi_{1.96}$ is ~2.7 W m^{-1} K^{-1}, but it is only ~0.8 W m^{-1} K^{-1} for $Yb_{0.7}Mg_{0.3}Mg_2Bi_{1.96}$, a reduction of ~70%. Benefiting from the greatly reduced thermal conductivity, the average ZT is effectively improved from ~0.46 for $YbMg_2Bi_{1.96}$ to ~0.61 for $Yb_{0.8}Mg_{0.2}Mg_2Bi_{1.96}$, an enhancement of ~33%.

Experimental

Synthesis

Ytterbium pieces (Yb, Sigma Aldrich, 99.9%, chunks), magnesium turnings (Mg, Sigma Aldrich, 99.9%, pieces), and bismuth ingots (Bi, Sigma Aldrich, 99.999%, chunks) were weighed according to the stoichiometry of $YbMg_2Bi_2$, $YbMg_2Bi_{1.98}$, and $Yb_{1-x}Mg_xMg_2Bi_{1.96}$ (x = 0, 0.1, 0.2, and 0.3) and loaded into a stainless-steel jar in a glovebox under argon atmosphere. The materials were ball-milled for 4 h by using a high energy ball mill (SPEX 8000D). The powders were then loaded into a graphite die with an inner diameter of 12.7 mm in a glovebox, and immediately sintered by alternating-current hot pressing at 933 K under pressure of ~80 MPa for 2 min. The hot-pressed disks are about 2-3 mm thick.

Characterization

A PANalytical multipurpose diffractometer with an X'celerator detector (PANalytical X'Pert Pro) was used to characterize the

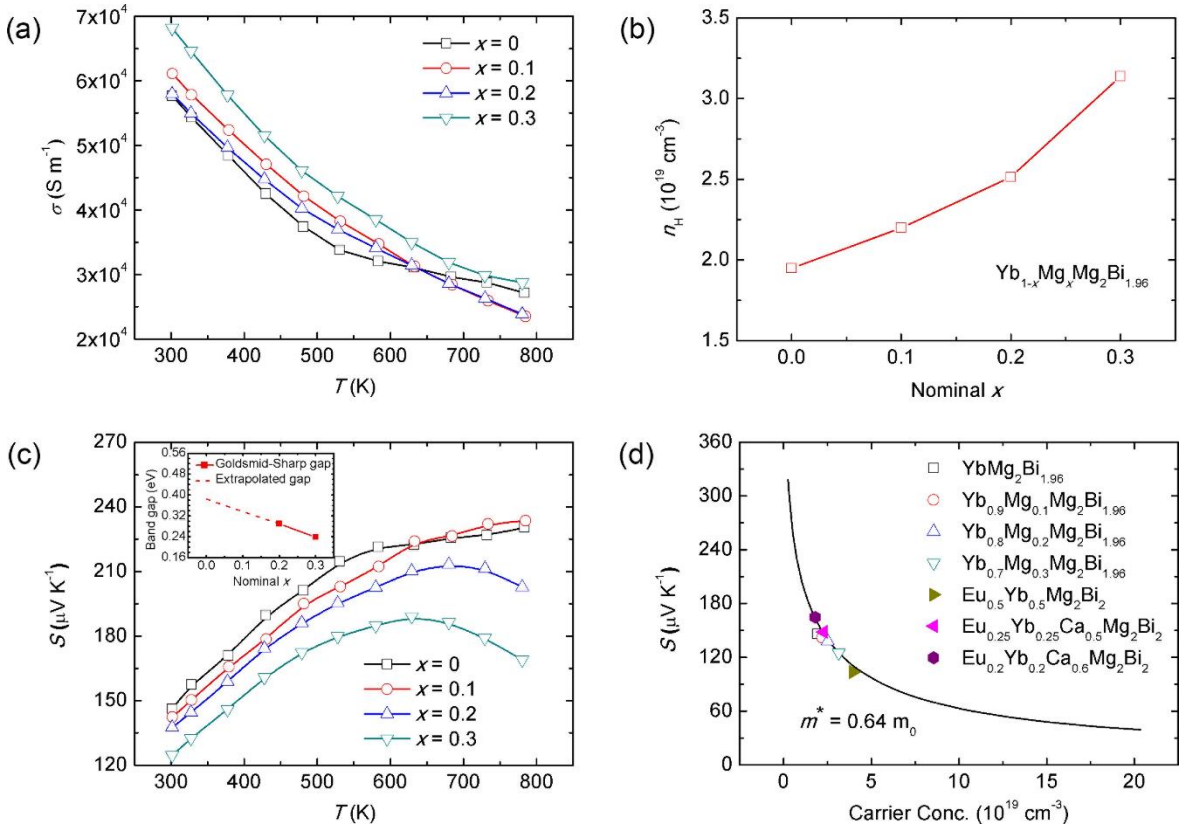

Fig. 2 (a) Temperature-dependent electrical conductivity, (b) composition-dependent Hall carrier concentration, and (c) temperature-dependent Seebeck coefficient of $Yb_{1-x}Mg_xMg_2Bi_{1.96}$ (x = 0, 0.1, 0.2, and 0.3); (d) Hall-carrier-concentration-dependent Seebeck coefficient of $Yb_{1-x}Mg_xMg_2Bi_{1.96}$ and previously studied compositions, including $Eu_{0.5}Yb_{0.5}Mg_2Bi_2$, $Eu_{0.25}Yb_{0.25}Ca_{0.5}Mg_2Bi_2$, and $Eu_{0.2}Yb_{0.2}Ca_{0.6}Mg_2Bi_2$.[43] The inset in (c) is the composition-dependent band gap of $Yb_{1-x}Mg_xMg_2Bi_{1.96}$ (x = 0.2 and 0.3 from the Goldsmid-Sharp formula and x = 0 and 0.1 extrapolated). The solid line in (d) is the calculated Pisarenko plot with m^* = 0.64 m_0 at room temperature.[12, 54, 55]

phase composition of the prepared samples. The morphology and elemental mapping of a representative sample were characterized by a scanning electron microscope (SEM) (LEO 1525) and energy-dispersive X-ray spectroscopy (JEOL 6340F), respectively. The electrical resistivity (ρ, $\rho=1/\sigma$) and Seebeck coefficient of the bar-shaped samples were simultaneously measured in a commercial system (ZEM-3, ULVAC) using the four-point direct current switching method. The total thermal conductivity was calculated using $\kappa_{total} = DC_p d$, where D (Fig. S1), C_p, and d (Table S1) are thermal diffusivity, specific heat capacity, and volume density, respectively. The thermal diffusivity (D) was measured using a laser flash apparatus (LFA 457, NETZSCH). The specific heat (C_p) was measured using a differential scanning calorimetry thermal analyzer (404 C, NETZSCH). The volumetric density (d) was determined by the Archimedean method. The room temperature Hall coefficient R_H was measured using a Physical Properties Measurement System (PPMS Dynacool, Quantum Design) with a magnetic field of 3 T and an electrical current of 8 mA. The Hall carrier concentration n_H was calculated by $n_H = 1/(eR_H)$.

Results and discussion

Fig. 1(a) shows the X-ray diffraction (XRD) patterns of the prepared $YbMg_2Bi_2$, $YbMg_2Bi_{1.98}$, and $Yb_{1-x}Mg_xMg_2Bi_{1.96}$ (x = 0, 0.1, 0.2, and 0.3). Except for the Bi-impurity phase (marked by a black arrow) in $YbMg_2Bi_2$ and $YbMg_2Bi_{1.98}$, all of the diffraction peaks can be indexed to the structure of $CaAl_2Si_2$ (space group $P\bar{3}m1$). The

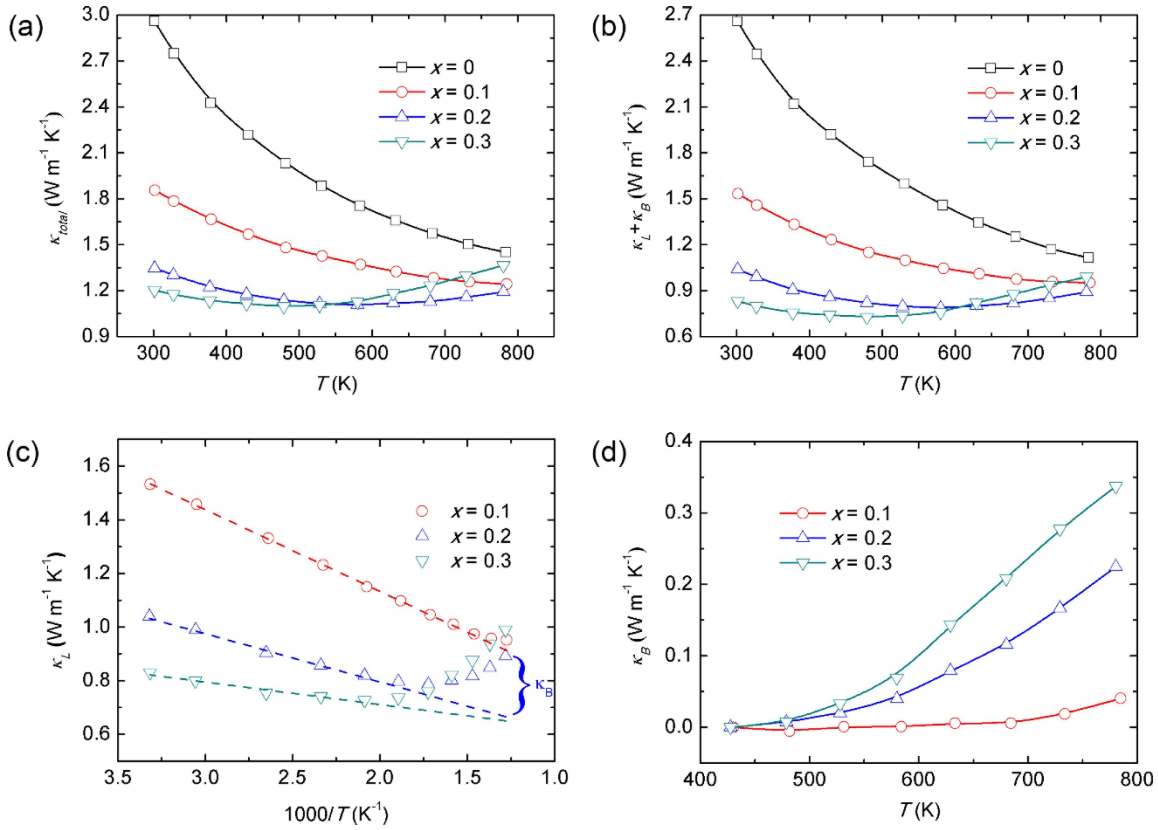

Fig. 3 Temperature-dependent (a) total thermal conductivity, (b) sum of lattice and bipolar thermal conductivity, (c) lattice thermal conductivity, and (d) bipolar thermal conductivity of $Yb_{1-x}Mg_xMg_2Bi_{1.96}$ (x = 0, 0.1, 0.2, and 0.3).

presence of the Bi-impurity phase should be due to the vaporization of Mg at elevated temperature. Additionally, the peaks shift to higher angles with increasing Mg content (Fig. 1(b)). To eliminate the Bi-impurity phase, we reduced the Bi content in the composition of $YbMg_2Bi_2$ to $YbMg_2Bi_{1.96}$. In this case, all of the diffraction peaks can be well indexed to the $CaAl_2Si_2$ crystal structure without the presence of secondary phases. We have also conducted the specific heat measurement, and the peak around 544 K (*i.e.*, the melting point of Bi) can be observed in both $YbMg_2Bi_2$ and $YbMg_2Bi_{1.98}$, but it disappears in all of the $Yb_{1-x}Mg_xMg_2Bi_{1.96}$ samples (Fig. 1(c)).[43] The lattice parameters of the $Yb_{1-x}Mg_xMg_2Bi_{1.96}$ solid solutions decrease monotonically with increasing Mg concentration (Fig. 1(d)), in good agreement with the Vegard's law. Such a reduction in the lattice parameters should be attributed to the smaller ionic radius of Mg^{2+} (65 pm) than that of Yb^{2+} (93 pm). The microstructure of a typical $Yb_{0.8}Mg_{0.2}Mg_2Bi_{1.96}$ sample (Fig. S2) shows homogeneous distribution of each element with no observable micro-holes, which indicates its high relative density. Therefore, it is clear that Mg successfully substitutes for Yb to form the $Yb_{1-x}Mg_xMg_2Bi_{1.96}$ solid solutions.

Fig. 2(a) shows the temperature-dependent electrical conductivity of $Yb_{1-x}Mg_xMg_2Bi_{1.96}$ samples. The electrical conductivity of $Yb_{1-x}Mg_xMg_2Bi_{1.96}$ decreases with the increasing temperature, showing the typical behavior of degenerated semiconductors. In addition, an increase in electrical conductivity can also be observed with increasing Mg content from x = 0 to x = 0.3, which should be ascribed to the increased Hall carrier concentration n_H (Fig. 2(b)). On one hand, this can be explained by the concentration of *A*-site defects in AB_2M_2 compounds[28], i.e. the Mg- and Yb-site defects in Mg_3Bi_2 and $YbMg_2Bi_2$, respectively. In fact, Mg is more electronegative than Yb. With increasing cation electronegativity, the defect formation enthalpy for cation vacancies decreases, which results in a smaller energy barrier for cation vacancy formation and an increasing amount of hole carrier concentration in the Mg_3Bi_2-$YbMg_2Bi_2$ solid solutions. On the other hand, the replacement of the isoelectronic cations with those of different electronegativity will lead to the variation in carrier

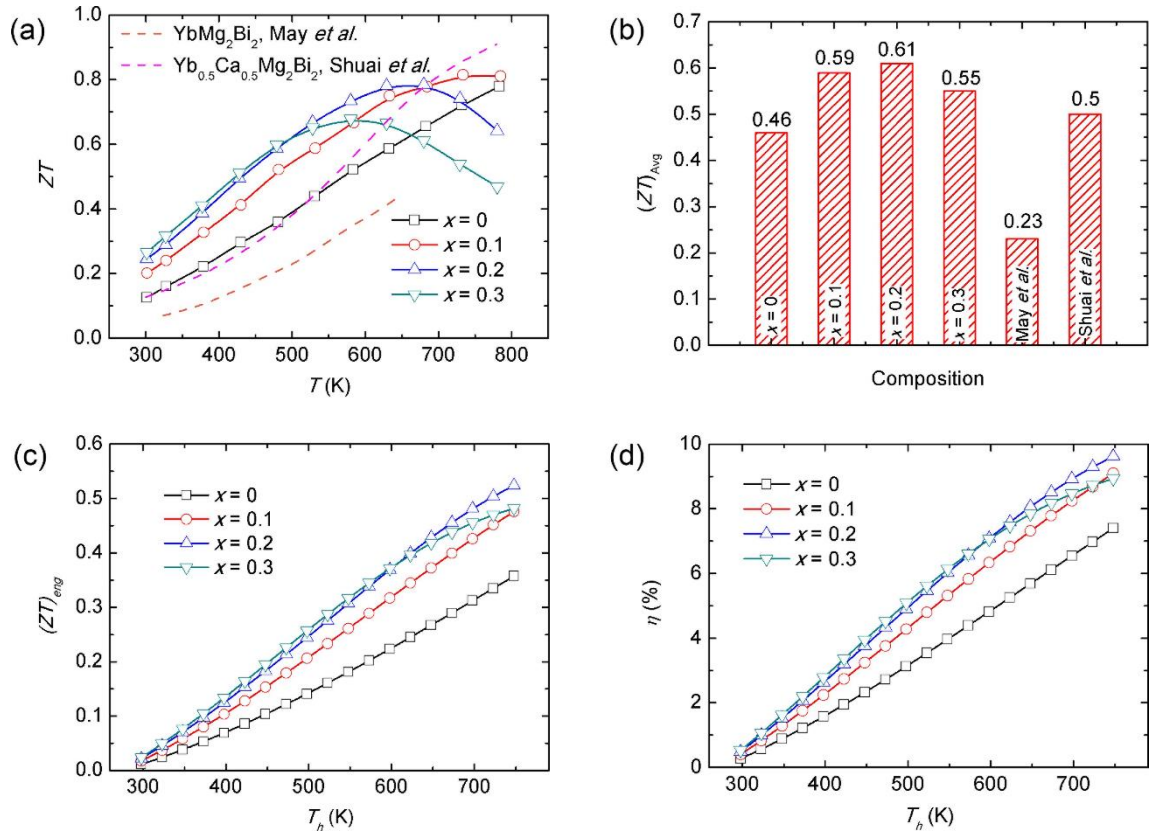

Fig. 4 (a) Temperature-dependent *ZT* values of $Yb_{1-x}Mg_xMg_2Bi_{1.96}$ (x = 0, 0.1, 0.2, and 0.3) in comparison with those of $YbMg_2Bi_2$[42] and $Yb_{0.5}Ca_{0.5}Mg_2Bi_2$;[44] (b) comparison of the average figure of merit among $Yb_{1-x}Mg_xMg_2Bi_{1.96}$ (x = 0, 0.1, 0.2, and 0.3) and results from May *et al.* and Shuai *et al.*; (c) calculated engineering figure of merit and (d) leg efficiency of $Yb_{1-x}Mg_xMg_2Bi_{1.96}$ (x = 0, 0.1, 0.2, and 0.3).

concentration.[56-59] Therefore, increasing the Mg concentration will increase the Hall carrier concentration in the p-type $Yb_{1-x}Mg_xMg_2Bi_{1.96}$ semiconductor.

Fig. 2(c) shows the temperature-dependent Seebeck coefficient of $Yb_{1-x}Mg_xMg_2Bi_{1.96}$ samples. Due to the variation in the Hall carrier concentration, the room-temperature Seebeck coefficient gradually decreases with the increasing Mg concentration. Fig. 2(d) shows the Pisarenko plot (Hall-carrier-concentration-dependent Seebeck coefficient) with $m^* = 0.64\ m_0$ at room temperature (see supplementary information for details). Similar to that of $Eu_{0.5}Yb_{0.5}Mg_2Bi_2$, $Eu_{0.25}Yb_{0.25}Ca_{0.5}Mg_2Bi_2$, and $Eu_{0.2}Yb_{0.2}Ca_{0.6}Mg_2Bi_2$ solid solutions, all of the current experimental data fall nearly completely on the fitting line, indicating that the valence band structure remains almost unchanged. In addition, it should be noted that the Seebeck coefficient of the samples with higher Mg concentration demonstrates a noticeable bipolar effect. This should be ascribed to the narrowing of the band gap, since Mg_3Bi_2 was reported to be a semi-metal (*i.e.*, with zero band gap). The band gap E_g can be analyzed by the Goldsmid–Sharp formula $E_g = 2e|S|_{max} T_{max}$, where e, S_{max}, and T_{max} are the electron charge, the maximum Seebeck coefficient, and the corresponding temperature, respectively.[60, 61] As shown in the inset of Fig. 2(c), E_g of the samples linearly decreases with increasing Mg content (the band gap among x = 0 and x = 0.1 is extrapolated from x = 0.2 and x = 0.3). As a consequence of the decreased E_g, it is obvious that the temperature corresponding to the maximum Seebeck coefficient for the samples shifts gradually from high to low temperature as the Mg content increases.

Fig. 3(a) shows the temperature-dependent κ_{total} of $Yb_{1-x}Mg_xMg_2Bi_{1.96}$ samples, where a substantial decrease in κ_{total} with increased Mg concentration can be observed. To clearly reveal the phonon scattering effect, the sum of lattice thermal conductivity κ_L and bipolar thermal conductivity κ_B is obtained by subtracting the electronic thermal conductivity κ_e ($\kappa_e = L\sigma T$, where L is the Lorenz number) from κ_{total}. The room temperature $\kappa_L+\kappa_B$ is ~2.7 W m^{-1} K^{-1} for $YbMg_2Bi_{1.96}$ and it is only ~0.9 W m^{-1} K^{-1} for $Yb_{0.7}Mg_{0.3}Mg_2Bi_{1.96}$, a decrease of 66% (Fig. 3(b)). Such a significant reduction in lattice thermal conductivity should be attributed to the substantial mass difference between the Yb (173.04 g mol^{-1}) and Mg (24.31 g mol^{-1}) atoms. In addition, it should be noted that the bipolar thermal conductivity at elevated temperature is substantially increased with the increase of Mg concentration in the higher temperature range (Fig. 3(d)) due to the decreased band gap, which is the same mechanism as reported for various compounds, such as PbTe,[62] $Ca_{1-x}Yb_xMg_2Bi_2$,[44] and Mg_2Sn–Mg_2Si–Mg_2Pb.[63]

According to the method proposed by Kitagawa *et al.*,[64] the contribution of bipolar thermal conductivity κ_B at higher temperature is roughly presented in Fig. 3(c) through separation from the total thermal conductivity κ_{total}. The dashed lines

represent a linearly fitted relationship between κ_L and T^{-1} over the temperature range from 300 to 773 K. The deviation of κ_L at higher temperature indicates the obvious bipolar thermal conductivity since the bipolar effect normally does not exist in the lower temperature range. As shown in Fig. 3(c) and (d), a slight κ_B deviation is initially observed for $Yb_{0.9}Mg_{0.1}Mg_2Bi_{1.96}$. As the Mg concentration is increased from x = 0.1 to x = 0.2 and x = 0.3, the κ_B significantly deviates from the linear relationship. This is due to the decreased band gap and therefore enhanced bipolar contribution with increasing Mg alloying concentration in $Yb_{1-x}Mg_xMg_2Bi_{1.96}$.

The dimensionless figure of merit ZT of $Yb_{1-x}Mg_xMg_2Bi_{1.96}$ is shown in Fig. 4(a). With the increasing temperature, ZTs increase monotonically in the lower temperature range. However, the ZTs of $Yb_{0.7}Mg_{0.3}Mg_2Bi_{1.96}$ and $Yb_{0.8}Mg_{0.2}Mg_2Bi_{1.96}$ decrease with temperature in the high temperature range due to the bipolar effect. This is in good agreement with the Seebeck coefficient and the thermal conductivity (Fig. 2(c) and Fig. 3). Benefiting from the significant decrease in thermal conductivity (especially at the lower temperature range), ZTs have been effectively improved for $Yb_{1-x}Mg_xMg_2Bi_{1.96}$ (x > 0). The room-temperature ZT is ~0.13 for $YbMg_2Bi_{1.96}$ but ~0.27 for $Yb_{0.7}Mg_{0.3}Mg_2Bi_{1.96}$, an increase of ~108%. At 773 K, the peak ZT can be ~0.8 for $Yb_{0.9}Mg_{0.1}Mg_2Bi_{1.96}$, due to the effectively reduced lattice thermal conductivity. In fact, the ZT values in the lower temperature range in our work are higher than those reported by May *et al.*[42] and Shuai *et al.*[44]

The average figure of merit $(ZT)_{avg}$ is calculated by the integration method over the temperature range from 300 to 773 K, as shown in Fig. 4(b). Samples alloyed with Mg show a noticeable increase in $(ZT)_{avg}$ compared to $YbMg_2Bi_{1.96}$. Due to the improved ZT in the lower temperature range, $(ZT)_{avg}$ is substantially improved from ~0.46 for $YbMg_2Bi_{1.96}$ to ~0.61 for $Yb_{0.8}Mg_{0.2}Mg_2Bi_{1.96}$, an enhancement of ~33%. In fact, since the engineering figure of merit $(ZT)_{eng}$ is a better evaluation of heat-to-electricity conversion efficiency for certain materials, we also calculated $(ZT)_{eng}$ and predicted the conversion efficiency (η) for $Yb_{1-x}Mg_xMg_2Bi_{1.96}$ based on eqns. (1)–(3):[65, 66]

$$(ZT)_{eng} = \frac{(PF)_{eng}}{\int_{T_c}^{T_h} \kappa(T)dT}(T_h - T_c) \quad (1)$$

$$(PF)_{eng} = \frac{\left(\int_{T_c}^{T_h} S(T)dT\right)^2}{\int_{T_c}^{T_h} \rho(T)d(T)} \quad (2)$$

$$\eta_{max} = \eta_c \frac{\sqrt{1+(ZT)_{eng}(\alpha_1/\eta_c)}-1}{\alpha_0\sqrt{1+(ZT)_{eng}(\alpha_1/\eta_c)}+\alpha_2}, \quad (3)$$

where S(T), ρ(T), and κ(T) are temperature-dependent thermoelectric properties, and α_i (i = 0, 1, and 2) is a dimensionless intensity factor of the Thomson effect. The hot-side temperature-dependent $(ZT)_{eng}$ and efficiency at the cold-side temperature of 323 K are shown in Fig. 4(c) and Fig. 4(d), respectively. It is clear that both $(ZT)_{eng}$ and efficiency increase with increasing Mg concentration from x = 0 to 0.2, with a slight decrease for x = 0.3 at high temperature. The peak $(ZT)_{eng}$ is ~0.35 for $YbMg_2Bi_{1.96}$ but ~0.55 for $Yb_{0.8}Mg_{0.2}Mg_2Bi_{1.96}$, an enhancement of ~57%. The peak efficiency is ~7.5% for $YbMg_2Bi_{1.96}$ but ~10% for $Yb_{0.8}Mg_{0.2}Mg_2Bi_{1.96}$, an increase of 33%.

Conclusions

In summary, solid solutions of $YbMg_2Bi_2$-Mg_3Bi_2 were prepared and studied. Significant point defect scattering between the Yb and Mg atoms effectively reduces the lattice thermal conductivity. As a result, a relatively high peak ZT of ~0.8 at 773 K can be achieved for $Yb_{0.9}Mg_{0.1}Mg_2Bi_{1.96}$. More importantly, a much higher $(ZT)_{avg}$ of ~0.61 can be obtained for $Yb_{0.8}Mg_{0.2}Mg_2Bi_{1.96}$, which is 33% higher than that of $YbMg_2Bi_{1.96}$.

Author contributions

Ting Zhou, Jun Mao, Chao Wang, and Zhifeng Ren designed research; Ting Zhou performed research; Jing Jiang, Shaowei Song, Hangtian Zhu, Qing Zhu, Qinyong Zhang, Wuyang Ren, and Zhiming Wang analyzed data; and Ting Zhou, Jun Mao, Chao Wang, and Zhifeng Ren wrote the paper.

Conflicts of interest

There are no conflicts to declare.

Acknowledgements

This work was supported by U.S. Department of Energy under Grant No. DE-SC0010831, the National Natural Science Foundation of China (Nos. 51672037, 61727818 and 61604031), the subproject of the National Key and Development Program of China (2017YFC0602102), the Department of Science and Technology of Sichuan Province (Nos. 2016JQ0022 and 2015JY0066), and the Open Foundation of National Engineering Research Center of Electromagnetic Radiation Control Materials (ZYGX2016K003-3). We thank T. Tong and Prof. J. M. Bao in the University of Houston, U.S., for analysing the band gap data.

References

1. F. J. DiSalvo, *Science*, 1999, **285**, 703-706.
2. L. E. Bell, *Science*, 2008, **321**, 1457-1461.
3. G. J. Snyder and E. S. Toberer, *Nature Materials*, 2008, **7**, 105-114.
4. J. Mao, Z. Liu, J. Zhou, H. Zhu, Q. Zhang, G. Chen and Z. Ren, *Advances in Physics*, 2018, **67**, 69-147.
5. O. Appel, M. Schwall, D. Mogilyansky, M. Köhne, B. Balke and Y. Gelbstein, *Journal of electronic materials*, 2013, **42**, 1340-1345.
6. C. Fu, T. Zhu, Y. Liu, H. Xie and X. Zhao, *Energy & Environmental Science*, 2015, **8**, 216-220.
7. J. Mao, J. Zhou, H. Zhu, Z. Liu, H. Zhang, R. He, G. Chen and Z. Ren, *Chemistry of Materials*, 2017, **29**, 867-872.
8. Y. Gelbstein, *Journal of electronic materials*, 2011, **40**, 533-536.

9. Y. Pei, Z. M. Gibbs, A. Gloskovskii, B. Balke, W. G. Zeier and G. J. Snyder, *Advanced energy materials*, 2014, **4**, 1400486-1400497.
10. F. Rosi, *Solid-State Electronics*, 1968, **11**, 833-868.
11. R. Vizel, T. Bargig, O. Beeri and Y. Gelbstein, *Journal of Electronic Materials*, 2016, **45**, 1296-1300.
12. E. S. Toberer, A. F. May and G. J. Snyder, *Chemistry of Materials*, 2010, **22**, 624-634.
13. J. Shuai, J. Mao, S. Song, Q. Zhang, G. Chen and Z. Ren, *Materials Today Physics*, 2017, **1**, 74-95.
14. S. M. Kauzlarich, S. R. Brown and G. J. Snyder, *Dalton transactions*, 2007, **21**, 2099-2107.
15. F. Gascoin, S. Ottensmann, D. Stark, S. M. Haïle and G. J. Snyder, *Advanced functional materials*, 2005, **15**, 1860-1864.
16. G. Miller and S. Kauzlarich, *VCH Publishers, New York*, 1996.
17. E. S. Toberer, S. R. Brown, T. Ikeda, S. M. Kauzlarich and G. Jeffrey Snyder, *Applied Physics Letters*, 2008, **93**, 062110.
18. S. R. Brown, S. M. Kauzlarich, F. Gascoin and G. J. Snyder, *Chemistry of materials*, 2006, **18**, 1873-1877.
19. J. F. Rauscher, C. A. Cox, T. Yi, C. M. Beavers, P. Klavins, E. S. Toberer, G. J. Snyder and S. M. Kauzlarich, *Dalton transactions*, 2010, **39**, 1055-1062.
20. S. R. Brown, E. S. Toberer, T. Ikeda, C. A. Cox, F. Gascoin, S. M. Kauzlarich and G. J. Snyder, *Chemistry of Materials*, 2008, **20**, 3412-3419.
21. H. Tamaki, H. K. Sato and T. Kanno, *Advanced materials*, 2016, **28**, 10182-10187.
22. J. Zhang, L. Song, S. H. Pedersen, H. Yin, L. T. Hung and B. B. Iversen, *Nature communications*, 2017, **8**, 13901-13908.
23. J. Mao, Y. Wu, S. Song, J. Shuai, Z. Liu, Y. Pei and Z. Ren, *Materials Today Physics*, 2017, **3**, 1-6.
24. J. J. Kuo, S. D. Kang, K. Imasato, H. Tamaki, S. Ohno, T. Kanno and G. J. Snyder, *Energy & Environmental Science*, 2018, **11**, 429-434.
25. T. Kanno, H. Tamaki, H. K. Sato, S. D. Kang, S. Ohno, K. Imasato, J. J. Kuo, G. J. Snyder and Y. Miyazaki, *Applied Physics Letters*, 2018, **112**, 033903-033907.
26. J. Mao, Y. Wu, S. Song, Q. Zhu, J. Shuai, Z. Liu, Y. Pei and Z. Ren, *ACS Energy Letters*, 2017, **2**, 2245-2250.
27. J. Mao, J. Shuai, S. Song, Y. Wu, R. Dally, J. Zhou, Z. Liu, J. Sun, Q. Zhang and C. dela Cruz, *Proceedings of the National Academy of Sciences*, 2017, **114**, 10548-10553.
28. G. S. Pomrehn, A. Zevalkink, W. G. Zeier, A. Van De Walle and G. J. Snyder, *Angewandte Chemie International Edition*, 2014, **53**, 3422-3426.
29. E. S. Toberer, A. F. May, B. C.Melot, E. Flage-Larsend and G. J. Snyder, *Dalton transactions*, 2009, **39**, 1046-1054.
30. Y. Takagiwa, Y. Sato, A. Zevalkink, I. Kanazawa, K. Kimura, Y. Isoda and Y. Shinohara, *Journal of Alloys and Compounds*, 2017, **703**, 73-79.
31. A. Zevalkink, W. G. Zeier, E. Cheng, J. Snyder, J.-P. Fleurial and S. Bux, *Chemistry of Materials*, 2014, **26**, 5710-5717.
32. M. Wood, U. Aydemir, S. Ohno and G. J. Snyder, *Journal of Materials Chemistry A*, 2018, **6**, 9437-9444.
33. X. Wang, M. Tang, H. Chen, X. Yang, J. Zhao, U. Burkhardt and Y. Grin, *Applied Physics Letters*, 2009, **94**, 092106-092108.
34. U. Aydemir, A. Zevalkink, A. Ormeci, Z. M. Gibbs, S. Bux and G. J. Snyder, *Chemistry of Materials*, 2015, **27**, 1622-1630.
35. U. Aydemir, A. Zevalkink, A. Ormeci, S. Bux and G. J. Snyder, *Journal of Materials Chemistry A*, 2016, **4**, 1867-1875.
36. E. S. Toberer, A. Zevalkink, N. Crisosto and G. J. Snyder, *Advanced Functional Materials*, 2010, **20**, 4375-4380.
37. A. Zevalkink, E. S. Toberer, T. Bleith, E. Flage-Larsen and G. J. Snyder, *Journal of Applied Physics*, 2011, **110**, 013721-013725.
38. A. Zevalkink, J. Swallow and G. J. Snyder, *Journal of Electronic Materials*, 2012, **41**, 813-818.
39. A. Zevalkink, G. S. Pomrehn, S. Johnson, J. Swallow, Z. M. Gibbs and G. J. Snyder, *Chemistry of Materials*, 2012, **24**, 2091-2098.
40. U. Aydemir, A. Zevalkink, A. Ormeci, H. Wang, S. Ohno, S. Bux and G. J. Snyder, *Dalton transactions*, 2015, **44**, 6767-6774.
41. A. F. May, M. A. McGuire, D. J. Singh, R. Custelcean and G. E. Jellison, Jr., *Inorganic chemistry*, 2011, **50**, 11127-11133.
42. A. F. May, M. A. McGuire, D. J. Singh, J. Ma, O. Delaire, A. Huq, W. Cai and H. Wang, *Physical Review B*, 2012, **85**, 035202-035211.
43. J. Shuai, H. Geng, Y. Lan, Z. Zhu, C. Wang, Z. Liu, J. Bao, C. W. Chu, J. Sui and Z. Ren, *Proceedings of the National Academy of Sciences of the United States of America*, 2016, **113**, E4125-4132.
44. J. Shuai, Z. Liu, H. S. Kim, Y. Wang, J. Mao, R. He, J. Sui and Z. Ren, *Journal of Materials Chemistry A*, 2016, **4**, 4312-4320.
45. J. Sun, J. Shuai, Z. Ren and D. J. Singh, *Materials Today Physics*, 2017, **2**, 40-45.
46. J. Shuai, H. S. Kim, Z. Liu, R. He, J. Sui and Z. Ren, *Applied Physics Letters*, 2016, **108**, 183901-183904.
47. D. Ramirez, A. Gallagher, R. Baumbach and T. Siegrist, *Journal of Solid State Chemistry*, 2015, **231**, 217-222.
48. R. He, H. Zhu, J. Sun, J. Mao, H. Reith, S. Chen, G. Schierning, K. Nielsch and Z. Ren, *Materials Today Physics*, 2017, **1**, 24-30.
49. Z. Liu, J. Mao, S. Peng, B. Zhou, W. Gao, J. Sui, Y. Pei and Z. Ren, *Materials Today Physics*, 2017, **2**, 54-61.
50. X. Shi, H. Kong, C. Li, C. Uher, J. Yang, J. Salvador, H. Wang, L. Chen and W. Zhang, *Applied Physics Letters*, 2008, **92**, 182101-182103.
51. Q. Zhang, B. Liao, Y. Lan, K. Lukas, W. Liu, K. Esfarjani, C. Opeil, D. Broido, G. Chen and Z. Ren, *Proceedings of the National Academy of Sciences*, 2013, **110**, 13261-13266.
52. L. Zhao, S. Lo, Y. Zhang, H. Sun, G. Tan, C. Uher, C. Wolverton, V. P. Dravid and M. G. Kanatzidis, *Nature*, 2014, **508**, 373-377.
53. L. Huang, Q. Zhang, Y. Wang, R. He, J. Shuai, J. Zhang, C. Wang and Z. Ren, *Physical Chemistry Chemical Physics*, 2017, **19**, 25683-25690.
54. G. Tan, W. G. Zeier, F. Shi, P. Wang, G. J. Snyder, V. P. Dravid and M. G. Kanatzidis, *Chemistry of Materials*, 2015, **27**, 7801-7811.
55. S. Airapetyants, M. Vinogradova, I. Dubrovskaya, N. Kolomoets and I. Rudnik, *SOVIET PHYS SOLID STATE*, 1966, **8**, 1069-1072.
56. W. Peng, S. Chanakian and A. Zevalkink, *Inorganic Chemistry Frontiers*, 2018, **5**, 1744-1759.
57. Y. Lu, S. Chen, W. Wu, Z. Du, Y. Chao and J. Cui, *Scientific reports*, 2017, **7**, 40224-40231.
58. Q. Cao, H. Zhang, M. Tang, H. Chen, X. Yang, Y. Grin and J. Zhao, *Journal of Applied Physics*, 2010, **107**, 053714-053718.
59. C. Yu, T. Zhu, S. Zhang, X. Zhao, J. He, Z. Su and T. M. Tritt, *Journal of Applied Physics*, 2008, **104**, 013705-013709.
60. H. Goldsmid and J. Sharp, *Journal of electronic materials*, 1999, **28**, 869-872.
61. Z. M. Gibbs, H.-S. Kim, H. Wang and G. J. Snyder, *Applied Physics Letters*, 2015, **106**, 022112-022116.
62. L. Zhao, H. Wu, S. Hao, C.-I. Wu, X. Zhou, K. Biswas, J. He, T. P. Hogan, C. Uher and C. Wolverton, *Energy & Environmental Science*, 2013, **6**, 3346-3355.

63. J. Mao, Y. Wang, B. Ge, Q. Jie, Z. Liu, U. Saparamadu, W. Liu and Z. Ren, *Physical Chemistry Chemical Physics*, 2016, **18**, 20726-20737.
64. H. Kitagawa, M. Wakatsuki, H. Nagaoka, H. Noguchi, Y. Isoda, K. Hasezaki and Y. Noda, *Journal of Physics and Chemistry of Solids*, 2005, **66**, 1635-1639.
65. W. Liu, J. Hu, S. Zhang, M. Deng, C.-G. Han and Y. Liu, *Materials Today Physics*, 2017, **1**, 50-60.
66. H. S. Kim, W. Liu, G. Chen, C.-W. Chu and Z. Ren, *Proceedings of the National Academy of Sciences*, 2015, **112**, 8205-8210.

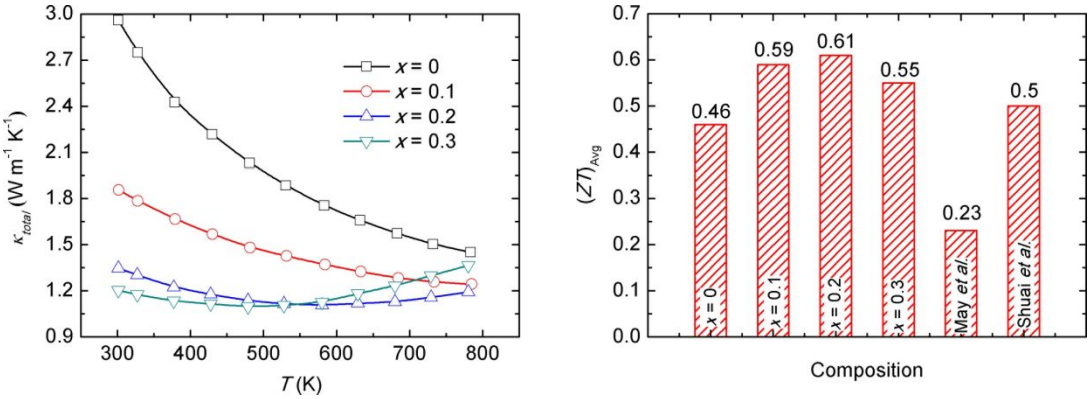

The thermoelectric property of $YbMg_2Bi_2$-Mg_3Bi_2 solid solution is studied.